Nanoscale

ROYAL SOCIETY OF CHEMISTRY

MINIREVIEW

View Article Online
View Journal | View Issue

Cite this: *Nanoscale*, 2020, **12**, 15036

Structure and performance of the $LiFePO_4$ cathode material: from the bulk to the surface

Jiangtao Hu, Weiyuan Huang, Luyi Yang * and Feng Pan *

Received 15th May 2020,
Accepted 23rd June 2020

DOI: 10.1039/d0nr03776a

rsc.li/nanoscale

Currently, $LiFePO_4$ is one of the most successfully commercialized cathode materials in the rechargeable lithium-ion battery (LIB) system, owing to its excellent safety performance and remarkable electrochemical properties and is expected to have a broader market in the near future. Although it is widely recognized that the crystalline structure of a cathode material largely dictates its electrochemical properties (*e.g.* capacity, cycle life and rate capabilities), this intrinsic connection in $LiFePO_4$ has not been systematically reviewed. Different from the previous reviews, which mainly focus on the improvement of electrochemical performance by all kinds of techniques, in this review, the relationship between its electrochemical performance and bulk/surface structure is reviewed and discussed. First, it is revealed that the intra-particle Li^+ transfer is influenced by several properties of the bulk, including crystalline structures, antisite defects and electronic structures. Next, it is demonstrated that the surface/interfacial structures of $LiFePO_4$, which can be reconstructed artificially or spontaneously, also have great impacts on the performances. Lastly, the intrinsic connection between the structure and performance is preliminarily established, showing brand-new perspectives on the strategy for further improvement and contributing to a comprehensive understanding of $LiFePO_4$.

1. Introduction

The cathode is regarded as a key component in lithium-ion batteries (LIBs) and the determinant of commercialization since it directly determines the electrochemical performance.[1–5] As the first-generation cathode material, layered oxide $LiCoO_2$ was commercialized with the C_6Li anode by Sony in 1991. Afterwards, other kinds of materials such as layered transition metal oxides ($LiNi_{1-y-z}Mn_yCo_zO_2$), Li-rich layered oxides, spinel oxides ($LiMn_2O_4$), polyanion oxides ($LiFePO_4$), *etc.*, have emerged in recent decades.[6–11] Despite the pursuit of high-energy-density battery materials, safety is still the paramount demand in battery systems for both portable electronic devices and electric vehicles (EVs). Therefore, demonstrating excellent safety features, $LiFePO_4$ has been the focus in both scientific research and the industrial community since the first report in 1997 by Goodenough *et al.*[12] Moreover,

School of Advanced Materials, Peking University Shenzhen Graduate School, Shenzhen 518055, China. E-mail: yangly@pkusz.edu.cn, panfeng@pkusz.edu.cn

Jiangtao Hu

Dr Jiangtao Hu received his Ph.D degree in 2013 from Peking University, China. His research interests mainly lie in design and development of functional materials for energy storage and conversion applications such as batteries, supercapacitors, and catalysis.

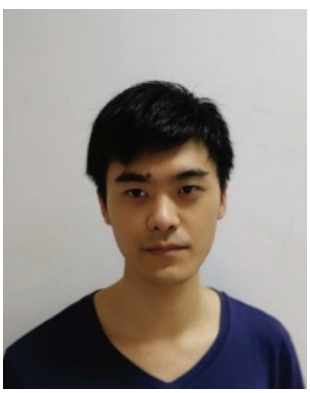

Weiyuan Huang

Weiyuan Hang received his B.S. degree in New Energy Materials and Devices from South China Normal University in 2017. He is pursuing his Ph.D. degree in the School of Advanced Materials, Peking University, China. His research interest includes energy storage and conversion applications including lithium ion batteries, sodium ion batteries, and supercapacitors.

its moderate operating voltage (3.5 V *vs.* Li/Li^+), moderate capacity (170 mA h g^{-1}), flat voltage plateau, abundant material supply, low material cost, and good environmental compatibility have also made $LiFePO_4$ a favourable cathode material for commercial LIBs. However, the poor electronic conductivity (>10^{-9} S cm^{-1}), low ionic diffusivity (*ca.* 10^{-11}–10^{-10} S cm^{-1}), poor low temperature performance and low volumetric energy density are considered main obstacles for its wider application.[13] To address these pressing issues, numerous works have been performed to investigate the synthesis, structure and defects of $LiFePO_4$, and important breakthroughs have been achieved and adopted by the market. Generally, the low ionic and electronic conductivities can be optimized by the following three methods: conductive layer coating,[14] element doping[13,15] and particle nanosizing.[16] As for the poor low temperature performance, optimizing the use of Li-salts, electrolyte solvents and additives can realize significant improvements;[17–19] moreover, reducing the particle size and removing the impurities in the raw materials are also deterministic ways to improve the low temperature performance.[20] To overcome the limitation of volumetric energy density, micro-sized $LiFePO_4$ particle preparation is the most common method, showing a porous structure for enhancing ionic and electronic conductivities.[21–23]

With decades of research and development of $LiFePO_4$, major breakthroughs have been made through various material modifications, playing an important role in solving the inherent drawbacks of $LiFePO_4$. Despite these exciting techniques and methods, it should still be noted that the electrochemical properties of $LiFePO_4$ can be essentially traced back to its crystalline structures. Moreover, as the confined region for the charge transfer process, the surface/interface structure of $LiFePO_4$ also dictates the reaction kinetics of $LiFePO_4$. Although many relevant studies have been carried out, they were not systematically summarized until now. In this review, the impact of the $LiFePO_4$ structure on its electrochemical performance will be briefly summarized from the bulk to the surface. With the aid of some graphical models, the mechanism of Li^+ diffusion is clearly presented, providing not only a better understanding of fundamental questions, but also useful guide on future material design.

2. Bulk structure of $LiFePO_4$

2.1 $LiFePO_4$ phase structure

Most cathode materials can be seen as crystals consisting of numerous basic structure units, which can be considered as "material genes" that assemble *via* periodic arrangement.[24] As a result, they directly determine most properties (*e.g.* Li^+ diffusion coefficient, thermal stability and electrochemical stability) of cathode materials. For instance, $LiFePO_4$ belongs to olivine family cathode materials with an orthorhombic lattice structure in a space group *Pnma*. Oxygen atoms in the structure are in hexagonal-close-packed arrangement, and phosphorus atoms and iron/lithium occupy tetrahedral and octahedral sites, which forms corner-shared FeO_6 octahedra and edge-shared LiO_6 octahedra parallel to the *b*-axis. The two octahedra are linked by the PO_4 tetrahedra, forming 3D spatial network structures, named α-$LiFePO_4$.[25] During delithiation, the $FePO_4$ phase appears in the single crystal structure, which has essentially the same crystalline structure as $LiFePO_4$ (Fig. 1). Up to the fully charged state, the volume change content is just 6.81%, which avoids capacity attenuation caused by volume changes during long-term cycles.[12] With the strong P–O covalent bond and limited volume variation, $LiFePO_4$ shows good thermal stability, cyclability and safety.

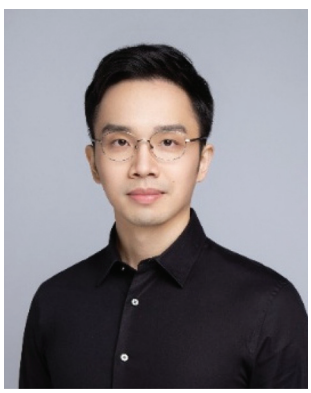

Luyi Yang

Dr Luyi Yang received his B.S. degree from the Department of Chemistry at Xiamen University (China) in 2010, and earned a Ph.D. degree from the School of Chemistry at Southampton University (U.K.) in 2015 under the supervision of Prof. John Owen. Dr Yang is currently a researcher at the School of Advanced Materials, Peking University Shenzhen Graduate School. His research interests mainly focus on the investigation of key materials in lithium batteries including solid-state electrolytes and cathode materials.

Feng Pan

Prof. Feng Pan, Chair-Professor, Founding Dean of School of Advanced Materials, Peking University Shenzhen Graduate School, and Director of National Center of Electric Vehicle Power Battery and Materials for International Research, received his B.S. degree from Dept. of Chemistry, Peking University, in 1985 and Ph.D. from Dept. of P&A Chemistry, University of Strathclyde, UK, with "Patrick D. Ritchie Prize" for the best Ph. D. in 1994. Prof. Pan has been engaged in fundamental research of structure chemistry, exploring "Material Genes" for Li-ion batteries and developing novel energy conversion-storage materials and devices. He also received the 2018 ECS Battery Division Technology Award.

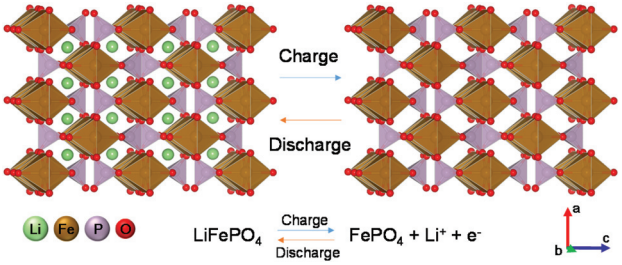

Fig. 1 Crystal structures of $LiFePO_4$ and $FePO_4$. During charging, $LiFePO_4$ changes to $FePO_4$ by delithiation. In the discharge process, a reversible transformation from $FePO_4$ to $LiFePO_4$ occurs by lithiation.

Two decades ago, another phase of $LiFePO_4$ (β-$LiFePO_4$) was synthesized under high pressure, exhibiting a space group of *Cmcm*.[26] Owing to the lower formation energy compared with α-$LiFePO_4$, β-$LiFePO_4$ is usually regarded as an intermediate or metastable state, and experiences a phase change from α to β at high temperatures.[27] In the *Cmcm* β-$LiFePO_4$ structure, tetrahedral LiO_4 shares a corner with the closed octahedral FeO_6 and a corner with the closed tetrahedral PO_4 (Fig. 2a). In this structure, Li^+ is isolated by the nearest FeO_6 and PO_4, leading to high energy barriers for lithium migration, which is why β-$LiFePO_4$ exhibits almost no electrochemical activity.[28] However, proper processing, such as introducing disorder structures and creating new diffusion channels in β-$LiFePO_4$, can also realize high capacity and stability[25] (Fig. 2b). Moreover, the factors that influence the controllable synthesis of β-$LiFePO_4$ were studied, which is helpful for us to obtain high performance olivine structure cathode materials.[29]

2.2 Antisite defects

Owing to the ordered-olivine structure, Li^+ moves in 1D diffusion channels, which can be easily blocked by Li/Fe disorder or stacking faults. Generally, a proper synthesis route and doping are effective approaches to suppress cation mixing and optimize the electrochemical performance. Guo *et al.*[30] synthesized $LiFePO_4$/carbon hybrid microtubes using strong chelation interaction with Fe^{3+} and absorption interaction with Li^+ of alginate, which yields very low Fe–Li antisite defects and exhibits remarkable electrochemical performance. Machida *et al.*[31] successfully realized O-site doping in $LiFePO_4$ by S, inducing an expanded lattice in a and b directions and suppression of antisite defects between Fe and Li owing to the larger ionic radius of S^{2-} than O^{2-}; hence, enhanced electrochemical properties were achieved. Furthermore, cation replacement (*e.g.* Nb-doping[32]) is another good way to improve the effective lithium mobility during the insertion/extraction reaction. Li diffusion in materials with a 1D diffusion mechanism, such as $LiFePO_4$, has a strong dependence on particle size, illustrating a significant reduction of Li diffusivity at large particle sizes. Moreover, if the antisite defects exist in the diffusion channels, the negative effects will be amplified. The correlation between the channel length and antisite content was built and described by Ceder's group[16] (Fig. 3a).

Ab initio molecular dynamics simulations prove that ionic migration perpendicular to the 1D channels has greater possibility than along the blocked channels by comparing the migration energy.[33] In addition, the related multi-dimensional transport properties have also been demonstrated in other studies.[34,35] The high dimensionality of ionic migration will be promoted by the support of channel crossover induced by high antisite content. $D_{[100]}$ and $D_{[001]}$ as a function of defect concentration were described, in which at 440 K, with higher defect concentration the Li^+ diffusivity decreases in the b direction and increases in the a and c directions (Fig. 3b). Pan *et al.*[36] synthesized α-$LiMn_{1-y}Fe_yPO_4$ with high antisite content, realizing excellent rate performance, which can be attributed to the 2D and/or 3D Li^+ diffusion mechanism, resulting in the transformation of the two-phase mechanism into a solid-state mechanism.

2.3 Special properties induced by the electronic structure

$LiFePO_4$ with an olivine structure exhibits long range antiferromagnetic order at low temperatures, below 51(1) K in $LiFePO_4$ and below 114(1) K in $FePO_4$.[37,38] The splitting of the d-orbitals in Fe^{2+} (d^5) and Fe^{3+} (d^6) will occur and form doubly degenerate e_g orbitals and triply degenerate t_{2g} orbitals. Through the electron transfer between Fe^{2+} and Fe^{3+} *via* the O 2p state exchange interaction can be realized and if both two ions are

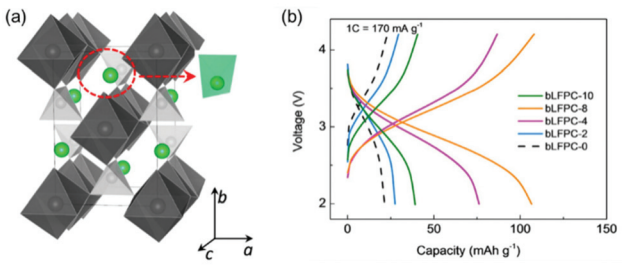

Fig. 2 (a) Crystal structure of β-$LiFePO_4$. Li^+ is shown in green, [FeO_6] octahedron is shown in dark gray, [PO_4] tetrahedron is shown in light gray, and [LiO_4] tetrahedron is shown in light green. (b) Electrochemical performance of β-$LiFePO_4$ with different ball-milling times. Reproduced from ref. 25 with permission from the American Chemical Society, copyright 2016.

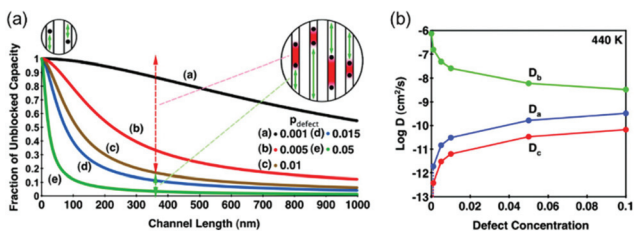

Fig. 3 (a) Expected unblocked capacity *vs.* channel length in $LiFePO_4$ for various defect concentrations. (b) Variation of the Li-vacancy self-diffusion $D_{[100]}$ (blue), $D_{[010]}$ (green), and $D_{[001]}$ (red) with the defect concentration at T = 440 K. Reproduced from ref. 16 with permission from the American Chemical Society, copyright 2010.

aligned ferromagnetically, then the ferromagnetical state emerges,[39] which has influences on the movement of charged particles. During the electrochemical process, Fe^{2+} and Fe^{3+} coexist in the bulk structure, bringing the possibility of the magnetic field interference on electrochemical properties. Pan *et al.*[40] provided strong proof about the relationship between magnetic domains and Li^+ diffusion, in which room temperature (RT) magnetic order was detected in Li_xFePO_4 ($x < 0.12$) nanocrystals, which trapped Li^+ and formed sub-10 nm solid solution domains owing to the strong Lorentz force in RT magnetic domains (Fig. 4). The formation of RT magnetic order was proposed due to both Fe^{2+}–Fe^{3+} super-exchange and the broken local symmetries induced by Fe^{2+}–Li^+ anti-site defects. Moreover, with the relationship between magnetic properties and element electronic structure, Werner *et al.* demonstrated a procedure to precisely determine the defect concentration by static magnetization measurements on $LiFePO_4$.[41] Under the hypothesis that the transition metals in $LiMn_{1-x}Fe_xPO_4$ are antiferromagnetic, the impact of the super-exchange interactions on the transition metal structure sequence and magnetic structure of $LiMn_{1-x}Fe_xPO_4$ was observed, suggesting the clustering arrangement of transition metals,[42] which explains the previous experimental results where $LiMn_{1-x}Fe_xPO_4$ generally exhibits two redox peaks, while sometimes only one can be observed.[43]

2.4 Other olivine-type cathode materials

Attempts have also been made to improve the energy density of $LiFePO_4$ by replacing Fe with other transition metals. $LiMnPO_4$ has also attracted researchers due to its higher voltage plateau at approximately 4 V *vs.* Li/Li^+. However, pristine $LiMnPO_4$ suffers from the mismatched $LiMnPO_4/MnPO_4$ interface and even poorer electronic conductivity which is several orders of magnitude lower than that of $LiFePO_4$.[44] Moreover, the Jahn–Teller distortion of unstable Mn^{3+} in charged $MnPO_4$ causes the deformation of the MnO_6 octahedra and Mn dissolution, and hence the capacity fading.[45,46] Alternatively, as the solid solution of $LiFePO_4$ and $LiMnPO_4$, $LiMn_{1-x}Fe_xPO_4$ exhibits two voltage plateaus, which correspond to Fe^{3+}/Fe^{2+} and Mn^{3+}/Mn^{2+} redox pairs. Similar to $LiFePO_4$ and $LiMnPO_4$, $LiMn_{1-x}Fe_xPO_4$ (LMFP) also exhibits low electronic and ionic conductivity. With high operating voltages, $LiNiPO_4$ (5.1 V *vs.* Li/Li^+) and $LiCoPO_4$ (4.8 V *vs.* Li/Li^+) are studied as potential cathode material candidates for high-energy-density batteries. However, they are both faced with not only low conductivity, but also poor chemical/electrochemical stabilities. One major issue is that their high operating voltages usually cause severe electrolyte degradation during the charging process. Different from $LiFePO_4$, $LiCoPO_4$ exhibits two voltage plateaus due to the formation of an intermediate $Li_{2/3}CoPO_4$ phase, which co-exists with both lithiated and delithiated phases.[47] However, the delithiated $CoPO_4$ is very unstable according to a first-principles calculation. Moreover, a second phase of Co_2P will be formed during heat treatment, which is detrimental to its capacity.[48] Compared with $LiCoPO_4$, $LiNiPO_4$ exhibits even worse cycle stability due to its higher charging voltage. Density functional theory (DFT) results also predict large volume changes (9.6%) between $LiNiPO_4$ and $NiPO_4$ during Li (de)intercalation, which induces structural instability.[49]

Inspired by the successful commercialization of $LiFePO_4$, iron phosphate has been tested as the host for other cations. With an acceptable theoretical capacity (154 mA h g^{-1}) and working potential (2.9 V *vs.* Na/Na^+), $NaFePO_4$ has been regarded as a promising alternative for $LiFePO_4$. Similar to $LiNiPO_4$, olivine $NaFePO_4$ also shows a different ion (de)intercalation mechanism to $LiFePO_4$, which includes a $Na_{2/3}FePO_4$ intermediate phase due to the volumetric mismatch between $NaFePO_4$ and $FePO_4$.[50] However, the theoretical capacity of $NaFePO_4$ cannot be fully realized in practice due to the poor electron conductivity and limited Na diffusion path. Therefore, one improvement strategy is to synthesize amorphous $NaFePO_4$.[51] Moreover, since olivine-phase $NaFePO_4$ exhibits lower thermodynamic stability compared to its maricite phase, which is electrochemically inert, it cannot be synthesized *via* traditional methods.[52] Other than Na-ions, Mg-ions can also be inserted into $FePO_4$ due to their similar ionic size to Li-ions. However, it is found that only half of the capacity can be achieved, which is due to that the Coulomb repulsions between Mg^{2+} in adjacent channels exert a large diffusion energy barrier for Mg-ion intercalation.[53]

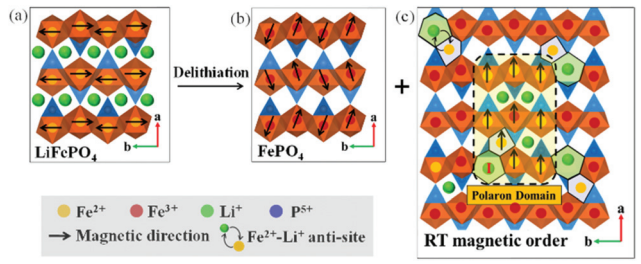

Fig. 4 Magnetic structures of $LiFePO_4$, $FePO_4$ and RT magnetic order zone. The magnetic polaron domain marked by a dashed black box, caused by the presence of antisite defects and super-exchange between Fe^{2+} and Fe^{3+}. Reproduced from ref. 40 with permission from the American Chemical Society, copyright 2019.

3. Surface electrochemistry of $LiFePO_4$

3.1 Artificial coating

Due to the poor ionic and electronic conductivity of $LiFePO_4$, surface engineering is a very common strategy to improve the electrochemical performance of $LiFePO_4$. A fast ion-conducting polyphosphate surface phase was obtained by Ceder's group,[54] which increases lithium ion diffusion across the surface; however, the final result is suspected by J. B. Goodenough *et al.*[55] As to the electronic conductivity, the coating substances include Cu, Ag, carbon, conducting polymers, metal oxides and polymers.[56–58] Among them, carbon coating attracts more

attention owing to its high conductivity, low lost, operation friendliness, and chemical stability during electrochemical processes.[59–61] Sun *et al.*[14] made a comprehensive summary on the development of carbon coating on $LiFePO_4$ cathode materials, related to carbon content, thickness, structure, morphology and porosity. In practical applications, the total carbon coating content and thickness should be optimized for high energy density $LiFePO_4$ LIBs. It has been previously revealed that enhancement of electronic conductivity and interparticle connectivity are the commonly held role of carbon coating;[62] however, it works more than that. Pan *et al.*[63] achieved an excess capacity of 186 and 207 mA h g^{-1} in $LiFePO_4$ samples (E-LFP) with mean particle sizes of 83 nm and 42 nm, respectively, by special carbon coating. The extra lithium was stored between the carbon layer and particles, which is a very stable structure built by C–O–Fe bonds, realizing full usage of the large surface areas of nanosized particles (Fig. 5).

As mentioned above, Mn, Co and Ni can be used to replace Fe for higher energy densities. However, severe interfacial degradation is a pressing challenge for these materials, which can be mitigated by artificial protective layers. By preparing a single-particle (SP) electrode, Yang and co-workers identified MnF_2 species on the surface of LMFP after cycling.[64] As shown in Fig. 6a, it is proposed that the Mn^{4+} generated by Mn^{3+} disproportionation will react with the solvent (*e.g.* EC) through a ring-opening process, forming $Mn(OR)_2$, which further combines with HF and eventually forms MnF_2 passivation domains, leading to capacity fading. The result also shows that Mn dissolution is more severe in the SP electrode compared to the conventional thick electrode due to the larger contact area between LMFP and the electrolyte. In order to suppress this surface degradation, a thin layer (approximately 5 nm) of Al_2O_3 is homogeneously applied on the cathode material *via* the atomic layer deposition (ALD) technique. It can be seen from Fig. 6b and c that after coating, the cycling stability of the LMFP single-particle electrode is greatly improved by inhibiting undesirable side reactions.

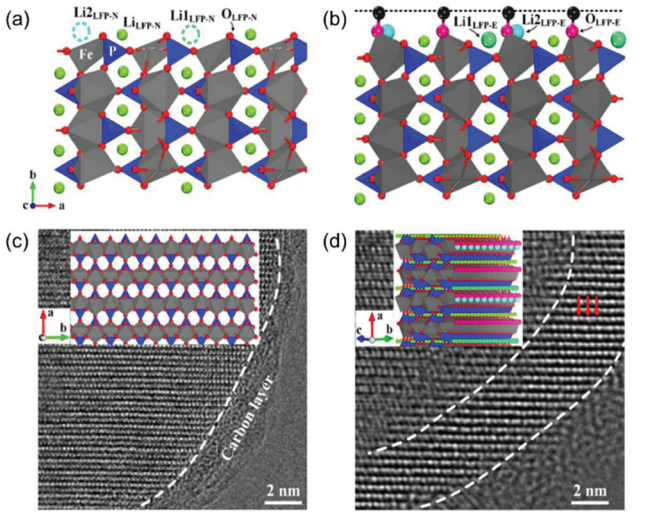

Fig. 5 (a, b) Crystal structures of normal $LiFePO_4$ (LFP-N) and excess capacity $LiFePO_4$ (LFP-E). (c, d) Transmission electron micrograph (TEM) of charged and discharged LFP-E nanoparticles, respectively. Reproduced from ref. 63 with permission from the American Chemical Society, copyright 2017.

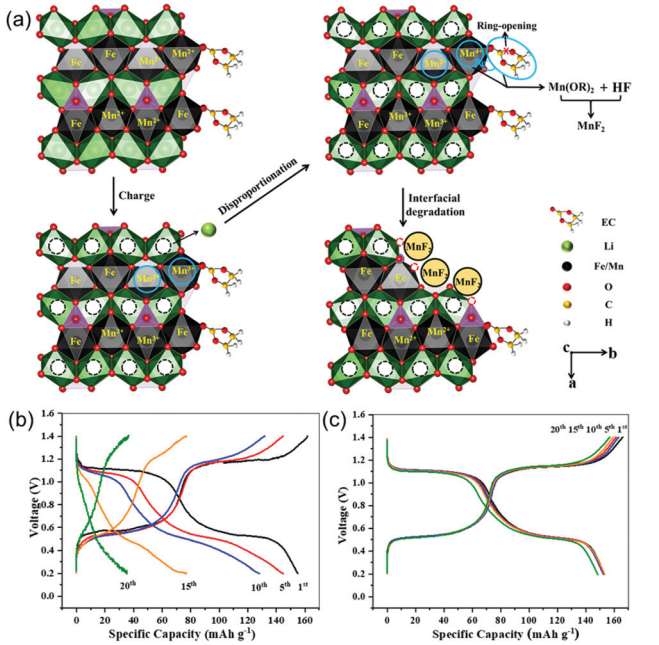

Fig. 6 (a) Proposed surface corrosion mechanism of LMFP particles; voltage profiles of different galvanostatic cycle numbers for (b) bare LMFP and (c) Al_2O_3 coated LMFP. Reproduced from ref. 64 with permission from the American Chemical Society, copyright 2019.

In order to avoid the direct contact between $LiCoPO_4$ and the electrolyte, Naoi and co-workers applied a layer of $FePO_4$ on the $LiCoPO_4$ surface.[65] Owing to the well-matched crystal structures, after coating, Fe^{3+} is found to partially diffuse to the bulk $LiCoPO_4$, forming an Fe-substituted $LiCoPO_4$ core with an Fe-rich outer layer. Such an outer layer is found to effectively suppress interfacial degradation reactions by exhibiting a capacity retention of as high as 99% after 100 cycles, which far surpasses that of the unmodified LCP materials.

Alternatively, concentration gradient hollow sphere $LiMn_{0.5}Fe_{0.5}PO_4$ with an Fe-rich surface and a Mn-rich core was synthesized by Wang and co-workers through a modified precipitation process (Fig. 7a).[66] In addition to higher chemical stability, the porous hollow structure could accommodate significant volume changes during repeated Li intercalation and deintercalation processes. As a result, a greatly improved cycle life was obtained (Fig. 7b). The higher discharge capacity of HCG-LMFP/C compared to C-LMFP/C is attributed to the high ionic/electric conductivity of the Fe-rich surface (Fig. 7b).

3.2 Spontaneous interfacial reconstruction

The solid–solution interface is an important part in cells, which is the gate for Li^+ in and out of the host materials. To

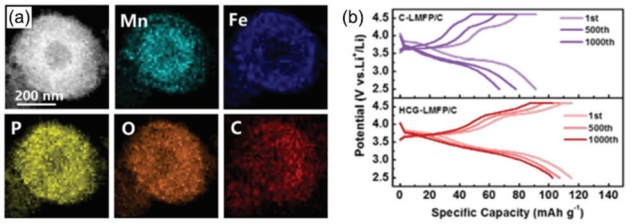

Fig. 7 (a) High-angle annular dark-field scanning TEM (HAADF-STEM) image and elemental mapping results from the cross-section of a hollow-structured concentration-gradient $LiMn_{0.5}Fe_{0.5}PO_4$/C (HCG-LMFP/C) particle. (b) Voltage profiles of a controlled $LiMn_{0.5}Fe_{0.5}PO_4$/C hollow sphere material (C-LMFP/C) and HCG-LMFP/C at 10C with 1000 cycles. Reproduced from ref. 66 with permission from the Royal Society of Chemistry, copyright 2019.

understand the impact of the interface on Li^+ transmission, its definition and structure should be clear. As is well-known, there is just physical contact between $LiFePO_4$ and carbon, which results in a loose structure with amounts of internal spaces, so the solvent molecules can permeate the carbon layer.[67] In the $LiFePO_4$ bulk, FeO_6 octahedra and LiO_6 octahedra were linked by the PO_4 tetrahedra and formed a perfect symmetry structure; however, in the $LiFePO_4$ and $FePO_4$ surface, it's a truncated octahedral symmetry. In this condition, how the Li^+ diffuses into the host material from the broken surface becomes very important and meaningful. Pan *et al.*[68] gave a perfect explanation both in aqueous and organic electrolytes (Fig. 8). By combining comprehensive electrochemistry tests and *ab initio* calculations, it was identified that the truncated symmetry of the solid $LiFePO_4$ surface could be compensated by the chemisorbed H_2O molecules or ethylene carbonate (EC) molecules, forming a half-solid ($LiFePO_4$) and half-liquid (H_2O or EC) Janus interface. This kind of interface promotes the Li desolvation process near the surface, realizing a super high rate performance, for example, in aqueous electrolyte at 600C (3600/600 = 6 s charge time, 1C = 170 mA h g^{-1}) reaching 72 mA h g^{-1} energy storage (42% of the theoretical capacity).

Rate performance[68] and cyclic voltammetry (CV) curves[69] of the $LiFePO_4$ electrode were also compared in aqueous and organic electrolytes. It was apparent that aqueous batteries exhibit higher rate performance and lower polarization. To investigate the mechanisms, while excluding the interference ionic transport between adjacent crystallites,[70] quasi-single-particle (QSP) $LiFePO_4$ electrodes and a QSP model were developed.[69] The prepared quasi monolayer electrodes consist of well separated single particles of $LiFePO_4$, which can minimize the concentration polarization, electrochemical polarization, and other internal interference to benefit for testing the intrinsic electrochemical properties of $LiFePO_4$. Through this model, the precise relationship between the reaction rate and voltage can be obtained by using the real potential-SOC curve of $LiFePO_4$. After the analysis of experimental and simulation results, Pan *et al.* found that the intrinsic Li^+ diffusion coefficients of $LiFePO_4$ are nearly the same in water and organic electrolytes, but the interfacial rate constant in aqueous electrolyte is one order higher, accounting for the excellent rate performance in aqueous electrolyte for $LiFePO_4$. It's also the first time of establishing the connection between the pre-exponential factor and Li^+ de-solvation/solvation process, that the larger the pre-exponential factor, the higher the interfacial rate constant and the faster the diffusivity.

With the previous work, it is known that surface reconstruction is important for Li^+ diffusion. To determine whether the above results have universal value owing to the complex electrolyte categories, Pan *et al.*[71] recently explored the effects of anions on surface reconstruction and the Helmholtz plane *vs.* lithium-ion transport at the solid–liquid interface (Fig. 9). Through *ab initio* calculations and comparison, it was proved that H_2O has a stronger binding energy with Fe and Li on the surface of $LiFePO_4$ and forms a Janus interface compared with different kinds of anions in aqueous electrolytes. Moreover,

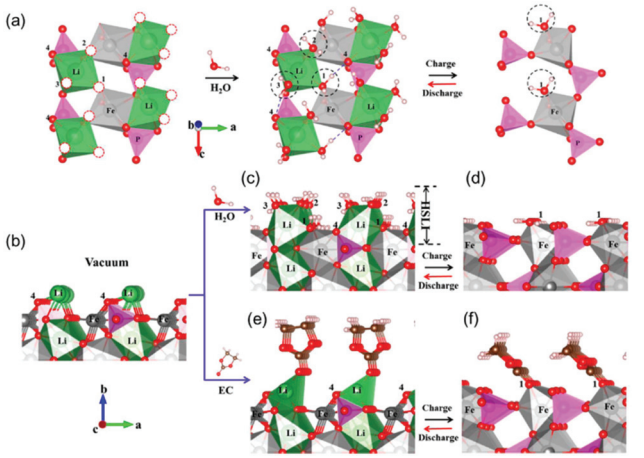

Fig. 8 *Ab initio* calculated H_2O/EC absorption at $LiFePO_4$ and $FePO_4$ surfaces. Reproduced from ref. 68 with permission from the American Chemical Society, copyright 2015.

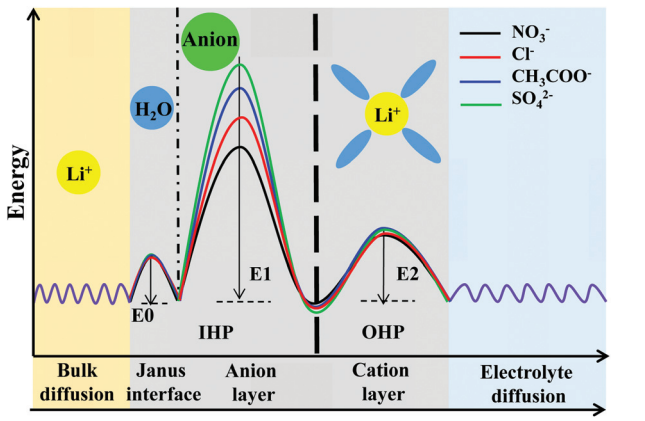

Fig. 9 The migration energy barrier of Li^+ in the inner Helmholtz plane (IHP) and outer Helmholtz plane (OHP). Reproduced from ref. 71 with permission from Elsevier, copyright 2020.

they divided the solid–liquid interface into three parts, which are the surface reconstruction layer (inner Helmholtz plane (IHP), E_0), anion adsorption layer (IHP, E_1) and cation adsorption layer (outer Helmholtz plane (OHP), E_2), and clearly illustrated the effects of the anion adsorption layer on Li^+ electrochemical behaviors.

4. Conclusions

To conclude, by illustrating the detailed bulk and surface structure information of $LiFePO_4$, its correlation with electrochemical performance is established. For the bulk structure, the effects of the phase structure, antisite defects and magnetic structure on performance have been reviewed, and all of these factors are closely related to Li^+ bulk diffusivity. (1) Owing to the high energy barriers for lithium migration, the synthesis conditions should be carefully controlled to avoid the presence of β-$LiFePO_4$. (2) Given that 2D and 3D Li^+ diffusion mechanisms could co-exist under the condition of high Fe^{2+}–Li^+ antisite content, a low-antisite route might not be necessary for achieving high diffusion ability. (3) Due to both Fe^{2+}–Fe^{3+} super-exchange and the broken local symmetries induced by Fe^{2+}–Li^+ antisite defects, RT magnetic order was induced, leading to the appearance of a solid–solution region and capacity loss.

As for the interface structure, three factors are included and analyzed. (1) The impact of electrolyte solvents on Li^+ interface kinetics. Taking an aqueous battery as an example, as shown in Fig. 10, the Li^+ diffusion pathway is presented. When Li^+ diffuses into the electrolyte from the anode, it will be coordinated by four water molecules in its primary solvation sheath, forming a complex cation $Li^+(H_2O)_4$. With the potential difference between the cathode and anode, the complex cation groups diffuse across the separator and into the cathode side. Close to the solid–liquid interface, $Li^+(H_2O)_4$ will shuffle off two H_2O and approach the $LiFePO_4$ surface, realizing particle surface reorganization by the left two H_2O. After Li^+ diffuses into the $LiFePO_4$ bulk along the Li channel, the connected two H_2O will desorb from the surface. By contrast, in the organic electrolyte, EC molecules will be bonded with Li^+, forming $Li^+(EC)_4$. Owing to its relatively bulky size, three EC molecules will be stripped off, bringing a much higher energy barrier when Li^+ crosses the interface, inducing a slower interfacial reaction constant compared with in the aqueous electrolyte. (2) The impact of the anion interfacial adsorption layer on Li^+ diffusion. The ionic absorption layer has a significant influence on Li^+ diffusion: the smaller the anion size, the better the diffusion ability. (3) Carbon coating affects the electronic conductivity and capacity. Carbon coating brought a breakthrough development of $LiFePO_4$, which realized a significant improvement of electron conductivity, achieving high capacity and rate performance. Moreover, with proper coating techniques, excess capacity could be realized for high energy density LIBs.[72] In actual applications, ionic conductivity is the determinant of performance owing to the lower diffusivity (*ca.* 10^{-11}–10^{-10} S cm^{-1} at RT) compared with electronic diffusivity (>10^{-9} S cm^{-1}), so the factors affecting ionic conductivity (*e.g.* size[73]) should be in good balance with carbon coating for realizing high energy-density and power-density LIBs.

Here, by establishing the relationship between the bulk–surface structure and the electrochemical performance, we aim to provide a new perspective on olivine-type $LiFePO_4$. However, the Li-ion diffusion behaviours at different states of charges and different places of a $LiFePO_4$ particle still remain unclear. Therefore, in the future, a deeper understanding is needed on the atomic scale to enable fast electron and ion transport. In addition, with the mature material preparing techniques and clear structural cognition, more attention should be paid to how to realize performance improvement under extreme environments, how to improve the volumetric energy density, and if there is a cost-effective synthetic route to produce a high-quality $LiFePO_4$ material.

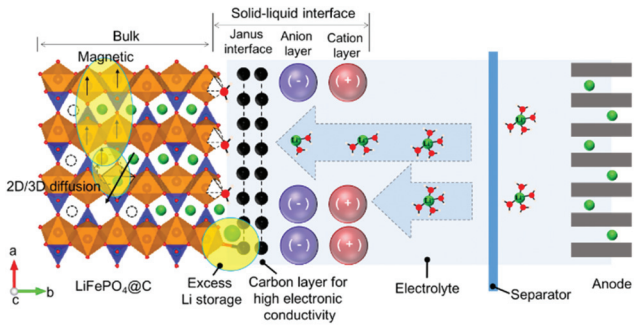

Fig. 10 Li^+ diffusion path from the electrolyte to the solid–liquid interface and then to $LiFePO_4$ bulk. The factors that affect the performance were concluded.

Conflicts of interest

There are no conflicts to declare.

Acknowledgements

This work was financially supported by the National Key R&D Program of China (2016YFB0700600), the National Natural Science Foundation of China (No. 21603007 and 51672012), and Shenzhen Science and Technology Research Grant (No. JCYJ20160531141048950 and JCYJ20150729111733470).

Notes and references

1 J.-T. Hu and J.-G. Zhang, *Chin. J. Struct. Chem.*, 2020, **38**, 2005–2008.
2 M.-J. Zhang, Y.-S. Chen, F. Pan and Y. Ren, *Chin. J. Struct. Chem.*, 2020, **39**, 26–30.
3 J. R. Owen, *Chem. Soc. Rev.*, 1997, **26**, 259–267.

4 Z. Chen, W. Zhang and Z. Yang, *Nanotechnology*, 2019, **31**, 012001.
5 L. Yang, K. Yang, J. Zheng, K. Xu, K. Amine and F. Pan, *Chem. Soc. Rev.*, 2020, DOI: 10.1039/d0cs00137f.
6 M. S. Whittingham, *Chem. Rev.*, 2014, **114**, 11414–11443.
7 T.-C. Liu, F. Pan and K. Amine, *Chin. J. Struct. Chem.*, 2020, **39**, 11–15.
8 Z. Zheng, M.-Y. Weng, L.-Y. Yang, Z.-X. Hu, Z.-F. Chen and F. Pan, *Chin. J. Struct. Chem.*, 2020, **38**, 2020–2026.
9 Z.-W. Yin, J.-T. Li, L. Huang, F. Pan and S.-G. Sun, *Chin. J. Struct. Chem.*, 2020, **39**, 20–25.
10 B. Pei, H. Yao, W. Zhang and Z. Yang, *J. Power Sources*, 2012, **220**, 317–323.
11 Q. Wang, W. Zhang, Z. Yang, S. Weng and Z. Jin, *J. Power Sources*, 2011, **196**, 10176–10182.
12 A. K. Padhi, K. S. Nanjundaswamy and J. B. Goodenough, *J. Electrochem. Soc.*, 1997, **144**, 1188–1194.
13 S.-Y. Chung, J. T. Bloking and Y.-M. Chiang, *Nat. Mater.*, 2002, **1**, 123–128.
14 J. Wang and X. Sun, *Energy Environ. Sci.*, 2012, **5**, 5163–5185.
15 B. Pei, Q. Wang, W. Zhang, Z. Yang and M. Chen, *Electrochim. Acta*, 2011, **56**, 5667–5672.
16 R. Malik, D. Burch, M. Bazant and G. Ceder, *Nano Lett.*, 2010, **10**, 4123–4127.
17 S. S. Zhang, K. Xu and T. R. Jow, *J. Power Sources*, 2006, **159**, 702–707.
18 X. Z. Liao, Z. F. Ma, Q. Gong, Y. S. He, L. Pei and L. J. Zeng, *Electrochem. Commun.*, 2008, **10**, 691–694.
19 L. Liao, X. Cheng, Y. Ma, P. Zuo, W. Fang, G. Yin and Y. Gao, *Electrochim. Acta*, 2013, **87**, 466–472.
20 N. Zhao, Y. Li, X. Zhao, X. Zhi and G. Liang, *J. Alloys Compd.*, 2016, **683**, 123–132.
21 H. Wang, R. Wang, L. Liu, S. Jiang, L. Ni, X. Bie, X. Yang, J. Hu, Z. Wang, H. Chen, L. Zhu, D. Zhang, Y. Wei, Z. Zhang, S. Qiu and F. Pan, *Nano Energy*, 2017, **39**, 346–354.
22 S. W. Oh, S. T. Myung, H. J. Bang, C. S. Yoon, K. Amine and Y. K. Sun, *Electrochem. Solid-State Lett.*, 2009, **12**, A181–185.
23 L. Wen, X. Hu, H. Luo, F. Li and H. Cheng, *Particuology*, 2015, **22**, 24–29.
24 J. Zheng, Y. Ye and F. Pan, *Natl. Sci. Rev.*, 2019, **2**, 242–245.
25 H. Guo, X. Song, Z. Zhuo, J. Hu, T. Liu, Y. Duan, J. Zheng, Z. Chen, W. Yang, K. Amine and F. Pan, *Nano Lett.*, 2016, **16**, 601–608.
26 O. García-Moreno, M. Alvarez-Vega, F. García-Alvarado, J. García-Jaca, J. M. Gallardo-Amores, M. L. Sanjuán and U. Amador, *Chem. Mater.*, 2001, **13**, 1570–1576.
27 G. Zeng, R. Caputo, D. Carriazo, L. Luo and M. Niederberger, *Chem. Mater.*, 2013, **25**, 3399–3407.
28 T. E. Ashton, J. V. Laveda, D. A. Maclaren, P. J. Baker, A. Porch, M. O. Jones and S. A. Corr, *J. Mater. Chem. A*, 2014, **2**, 6238–6245.
29 H. Guo, H. Ping, J. Hu, X. Song, J. Zheng and F. Pan, *J. Mater. Chem. A*, 2017, **5**, 14294–14300.
30 Y. Zou, S. Chen, X. Yang, N. Ma, Y. Xia, D. Yang and S. Guo, *Adv. Energy Mater.*, 2016, **6**, 1601549.
31 K. Okada, I. Kimura and K. Machida, *RSC Adv.*, 2018, **8**, 5848–5853.
32 S. Y. Chung, S. Y. Choi, T. Yamamoto and Y. Ikuhara, *Angew. Chem., Int. Ed.*, 2009, **48**, 543–546.
33 J. Yang and J. S. Tse, *J. Phys. Chem. A*, 2011, **115**, 13045–13049.
34 R. Amin, J. Maier, P. Balaya, D. P. Chen and C. T. Lin, *Solid State Ionics*, 2008, **179**, 1683–1687.
35 G. R. Gardiner and M. S. Islam, *Chem. Mater.*, 2010, **22**, 1242–1248.
36 J. Hu, Y. Xiao, H. Tang, H. Wang, Z. Wang, C. Liu, H. Zeng, Q. Huang, Y. Ren, C. Wang, W. Zhang and F. Pan, *Nano Lett.*, 2017, **17**, 4934–4940.
37 N. A. Chernova, G. M. Nolis, F. O. Omenya, H. Zhou, Z. Li and M. S. Whittingham, *J. Mater. Chem.*, 2011, **21**, 9865–9875.
38 G. Rousse, J. Rodriguez-Carvajal, S. Patoux and C. Masquelier, *Chem. Mater.*, 2003, **15**, 4082–4090.
39 A. Mauger, K. Zaghib, F. Gendron and C. M. Julien, *Ionics*, 2008, **14**, 209–214.
40 J. Hu, H. Zeng, X. Chen, Z. Wang, H. Bin Wang, R. Wang, L. Wu, Q. Huang, L. Kong, J. Zheng, Y. Xiao, W. Zhang and F. Pan, *J. Phys. Chem. Lett.*, 2019, **10**, 4794–4799.
41 J. Werner, C. Neef, C. Koo, S. Zvyagin, A. Ponomaryov and R. Klingeler, *arXiv*, 2020, **220**, 1–15.
42 Y. Liu, Y. Gu, H. Zeng, J. Zheng and F. Pan, *J. Phys. Chem. C*, 2019, **123**, 17002–17009.
43 A. Paolella, G. Bertoni, E. Dilena, S. Marras, A. Ansaldo, L. Manna and C. George, *Nano Lett.*, 2014, **14**, 1477–1483.
44 C. Delacourt, L. Laffont, R. Bouchet, C. Wurm, J.-B. Leriche, M. Morcrette, J.-M. Tarascon and C. Masquelier, *J. Electrochem. Soc.*, 2005, **152**, A913.
45 Z. Zhuo, J. Hu, Y. Duan, W. Yang and F. Pan, *Appl. Phys. Lett.*, 2016, **109**, 1–6.
46 Y. Deng, C. Yang, K. Zou, X. Qin, Z. Zhao and G. Chen, *Adv. Energy Mater.*, 2017, **7**, 1601958.
47 M. Zhang, N. Garcia-Araez and A. L. Hector, *J. Mater. Chem. A*, 2018, **6**, 14483–14517.
48 J. Wolfenstine, J. Read and J. L. Allen, *J. Power Sources*, 2007, **163**, 1070–1073.
49 C. Li, X. Miao, W. Chu, P. Wu and D. G. Tong, *J. Mater. Chem. A*, 2015, **3**, 8265–8271.
50 M. Casas-Cabanas, V. V. Roddatis, D. Saurel, P. Kubiak, J. Carretero-González, V. Palomares, P. Serras and T. Rojo, *J. Mater. Chem.*, 2012, **22**, 17421–17423.
51 C. Li, X. Miao, W. Chu, P. Wu and D. G. Tong, *J. Mater. Chem. A*, 2015, **3**, 8265–8271.
52 J. Lu, S. C. Chung, S. I. Nishimura and A. Yamada, *Chem. Mater.*, 2013, **25**, 4557–4565.
53 P. Shan, Y. Gu, L. Yang, T. Liu, J. Zheng and F. Pan, *Inorg. Chem.*, 2017, **56**, 13411–13416.
54 B. Kang and G. Ceder, *Nature*, 2009, **458**, 190.
55 K. Zaghib, J. B. Goodenough, A. Mauger and C. Julien, *J. Power Sources*, 2009, **194**, 1021–1023.
56 F. Croce, A. D'Epifanio, J. Hassoun, A. Deptula, T. Olczac and B. Scrosati, *Electrochem. Solid-State Lett.*, 2002, **5**, 47–50.

57 Y. Jin, C. P. Yang, X. H. Rui, T. Cheng and C. H. Chen, *J. Power Sources*, 2011, **196**, 5623–5630.
58 Y. H. Huang and J. B. Goodenough, *Chem. Mater.*, 2008, **20**, 7237–7241.
59 L.-L. Jia, Y.-C. Ji, K. Yang, Z.-J. Wang, H.-B. Chen and F. Pan, *Chin. J. Struct. Chem.*, 2020, **39**, 200–205.
60 R. Dominko, M. Bele, M. Gaberscek, M. Remskar, D. Hanzel, S. Pejovnik and J. Jamnik, *J. Electrochem. Soc.*, 2005, **152**, A607.
61 S. W. Oh, S. T. Myung, S. M. Oh, K. H. Oh, K. Amine, B. Scrosati and Y. K. Sun, *Adv. Mater.*, 2010, **22**, 4842–4845.
62 N. Ravet, Y. Chouinard, J. F. Magnan, S. Besner, M. Gauthier and M. Armand, *J. Power Sources*, 2001, **97–98**, 503–507.
63 Y. Duan, B. Zhang, J. Zheng, J. Hu, J. Wen, D. J. Miller, P. Yan, T. Liu, H. Guo, W. Li, X. Song, Z. Zhuo, C. Liu, H. Tang, R. Tan, Z. Chen, Y. Ren, Y. Lin, W. Yang, C. M. Wang, L. W. Wang, J. Lu, K. Amine and F. Pan, *Nano Lett.*, 2017, **17**, 6018–6026.
64 W. Huang, J. Hu, L. Yang, W. Zhao, Z. Wang, H. Wang, Z. Guo, Y. Li, J. Liu, K. Yang and F. Pan, *ACS Appl. Mater. Interfaces*, 2019, **11**, 957–962.
65 N. Okita, E. Iwama, Y. Takami, S. Abo, W. Naoi, M. Thomas, H. Reid and K. Naoi, *Electrochemistry*, 2019, **87**, 156–161.
66 T. Ruan, B. Wang, F. Wang, R. Song, F. Jin, Y. Zhou, D. Wang and S. Dou, *Nanoscale*, 2019, **11**, 4073–4082.
67 K. Zaghib, M. Dontigny, P. Charest, J. F. Labrecque, A. Guerfi, M. Kopec, A. Mauger, F. Gendron and C. M. Julien, *J. Power Sources*, 2008, **185**, 698–710.
68 J. Zheng, Y. Hou, Y. Duan, X. Song, Y. Wei, T. Liu, J. Hu, H. Guo, Z. Zhuo, L. Liu, Z. Chang, X. Wang, D. Zherebetskyy, Y. Fang, Y. Lin, K. Xu, L. W. Wang, Y. Wu and F. Pan, *Nano Lett.*, 2015, **15**, 6102–6109.
69 J. Hu, W. Li, Y. Duan, S. Cui, X. Song, Y. Liu, J. Zheng, Y. Lin and F. Pan, *Adv. Energy Mater.*, 2017, **7**, 1601894.
70 K. T. Lee, W. H. Kan and L. F. Nazar, *J. Am. Chem. Soc.*, 2009, **131**, 6044–6045.
71 J. Hu, W. Ren, X. Chen, Y. Li, W. Huang, K. Yang, L. Yang, Y. Lin, J. Zheng and F. Pan, *Nano Energy*, 2020, **74**, 104864.
72 C. Lu, X. Jiang, W. Sun, Z. Wang, K. Sun, D. W. Rooney and J. Wang, *J. Mater. Chem. A*, 2017, **5**, 24636–24644.
73 M. Gaberscek, R. Dominko and J. Jamnik, *Electrochem. Commun.*, 2007, **9**, 2778–2783.